ICOSSAR 2021
The 13th International Conference on Structural Safety and Reliability (ICOSSAR 2021), June 21-25, 2021, Shanghai, P.R. China
J. Li, Pol D. Spanos, J.B. Chen & Y.B. Peng (Eds)

Efficient Sampling Techniques for Simulation-based Life-Cycle Structural Reliability and Seismic Fragility Assessment

Luca Capacci and Fabio Biondini

Department of Civil and Environmental Engineering, Politecnico di Milano, Milan, Italy

ABSTRACT: Life-cycle structural reliability assessment and risk analysis of deteriorating systems may involve the modeling of complex time-variant probabilistic processes. Although simulation methods are frequently the only viable tools to solve this kind of problems, they are time-consuming and might be computationally inefficient and unfeasible in practice if small probabilities of failure need to be estimated, particularly for large-scale reliability and risk analysis problems. To mitigate the computational effort of simulation methods in estimating the time-variant failure probability of deteriorating structures, a novel computational approach based on Importance Sampling and clustering-based data reduction techniques is proposed. The computational efficiency of the proposed methodology is demonstrated with practical applications to life-cycle reliability and seismic fragility of reinforced concrete structures exposed to corrosion.

KEYWORDS: Life-Cycle Reliability; Seismic Fragility; Simulation; Importance Sampling; Data Clustering.

1 INTRODUCTION

Reliability assessment and fragility analysis of structural systems should account for the effects of aging and deterioration processes that may adversely affect the system performance over time (Biondini and Frangopol 2016). To this aim, the time evolution of the uncertainty effects must be properly considered since the impact of aleatory and epistemic uncertainties can be exacerbated by lifetime degradation of materials and components (Ellingwood 2005). Therefore, structural performance metrics should be formulated as time-variant probabilistic indicators (Ghosn et al. 2016). However, the effective incorporation of such effects into structural reliability assessment and fragility analysis frameworks can be challenging for large-scale structural systems and infrastructure networks (Silva *et al.* 2019).

In this paper, a novel computationally efficient approach is proposed for the time-variant structural reliability assessment and fragility analysis (Capacci 2020, Capacci and Biondini 2021). This approach is based on importance sampling and clustering techniques accounting for the time-variant formulation of the problem. The sample structural systems to be analyzed in the simulation process are efficiently selected to account for the time-variant modeling of uncertainties that are inherent to life-cycle structural reliability assessment and fragility analysis.

The proposed methodology is applied in comparison with crude Monte Carlo simulation for probabilistic lifetime seismic response of reinforced concrete (RC) bridges exposed to corrosion processes. Then, reliability estimates are defined by weighting each failed sample based on their time-variant likelihood of occurrence. The calibration of time-variant seismic fragility curves is also investigated for different limit states, from damage limitation up to structural collapse, based on multi-stripe dynamic analysis.

2 TIME-VARIANT RELIABILITY AND SEISMIC FRAGILITY

2.1 *Lifetime structural reliability*

The probability of failure $p_{f,s}$ and reliability index $\beta = \Phi^{-1}(1 - p_{f,s})$ associated with the attainment of the s-th limit state of a structural system can be formulated based on a safety factor $\Theta_s(\mathbf{Z})\leq 1$ expressed as a function of a set of random variables $\mathbf{Z}$ that characterize the structural problem:

$$p_{f,s} = P[\Theta_s(\mathbf{Z}) \leq 1] = \int_{\mathbf{z}} I[\Theta_s(\mathbf{z}) \leq 1] \cdot f_{\mathbf{Z}}(\mathbf{z}) d\mathbf{z} \quad (1)$$

where $f_{\mathbf{Z}}(\mathbf{z})$ is the joint probability density function (PDF) of $\mathbf{Z}$.

The indicator function $I[\Theta_s(\mathbf{Z})\leq 1]$ is a Heaviside step function equal to 1 in the failure domain and 0 otherwise. For the sake of formal synthesis, the indicator function will be expressed using the following notation:

$$I_s[\mathbf{z}] = I[\Theta_s(\mathbf{z}) \leq 1] \quad (2)$$

The time-variant failure probability is expressed with respect to the random processes $\mathbf{Z}(t)$ generated based on time-variant deterioration processes $\mathbf{\Delta}(t)$ and time-invariant basic structural model random variables $\mathbf{K}$, (e.g., material mechanical properties, structural geometry, etc.). Furthermore, deterioration processes $\mathbf{\Delta}(t)$ are generally determined as a function of environmental hazard parameters $\mathbf{H}_e$ (e.g., concentration of aggressive chemical components, material permeability, etc.):

$$\mathbf{Z}(t) = \mathbf{Z}[\mathbf{K}, \mathbf{\Delta}(\mathbf{H}_e; t)] \quad (3)$$

2.2 *Time-variant seismic fragility*

Seismic fragility analysis of a structural system provides the exceedance probability of safety conditions under earthquakes of given intensity, representing in probabilistic terms the capacity to sustain a prescribed seismic demand. In the following, fragility curves are defined as the exceedance probability of a prescribed damage state s_b under a seismic intensity i_b (Capacci 2020):

$$p_{f,s}(i_b) = P[S_b \geq s_b | i_b] \quad (4)$$

where S_b is a discrete random variable indicating the damage level suffered by the structure among the set of possible states.

Analytical fragility curves rely on a direct relationship between seismic actions and the effects on the mechanical response of structural systems. The time-variant exceedance probability $p_{f,s}$ of a given damage state s_b for a prescribed seismic intensity i_b can be formulated as follows:

$$p_{f,s}(i_b, t) = \int_{\mathbf{z}} I_s[\mathbf{z}(t)|i_b] \cdot f_{\mathbf{Z}(t)}(\mathbf{z}) d\mathbf{z} \quad (5)$$

3 SIMULATION-BASED TECHNIQUES

3.1 *Monte Carlo simulation*

Monte Carlo Simulation (MCS) is a versatile tool for the numerical solution of multidimensional integrals based on the artificial generation of n_j samples of the basic variables constituting the model uncertainties. Figure 1a shows a flowchart of crude MCS applied to life-cycle seismic fragility assessment. MCS allows estimating the expected value of the indicator function in the failure region, which corresponds to the failure probability:

$$\hat{p}_{\mathrm{MCS}}(t) = \frac{1}{n_j} \sum_{j=1}^{n_j} I_s[\mathbf{z}_j(t)] \quad (6)$$

where outcomes of the stochastic processes $\mathbf{z}_j$ are simulated based on outcomes of the basic random variables of both the structural model $\mathbf{\kappa}_j$ and environmental hazard $\mathbf{\eta}_{e,j}$:

$$\mathbf{z}_j(t) = \mathbf{z}\left(\mathbf{\kappa}_j, \mathbf{\delta}_j\left(\mathbf{\eta}_{e,j}; t\right)\right) \quad (7)$$

The sample deterioration process $\mathbf{\delta}_j(t_k)$ is usually generated at different time instants $t=t_k$ with $k=1,\ldots,n_t$ based on the simulation of the environmental hazard parameters $\mathbf{\eta}_{e,j}$. Then, the simulation of the basic variables $\mathbf{\kappa}_j$ leads to characterize the sample models $\mathbf{z}_j(t_k)$ and, finally, to carry out structural analysis to numerically estimate the failure probability at the prescribed time instants t_k.

One of the main drawbacks of crude MCS is that a large sample size is often needed to attain sufficiently accurate estimates for small failure probabilities.

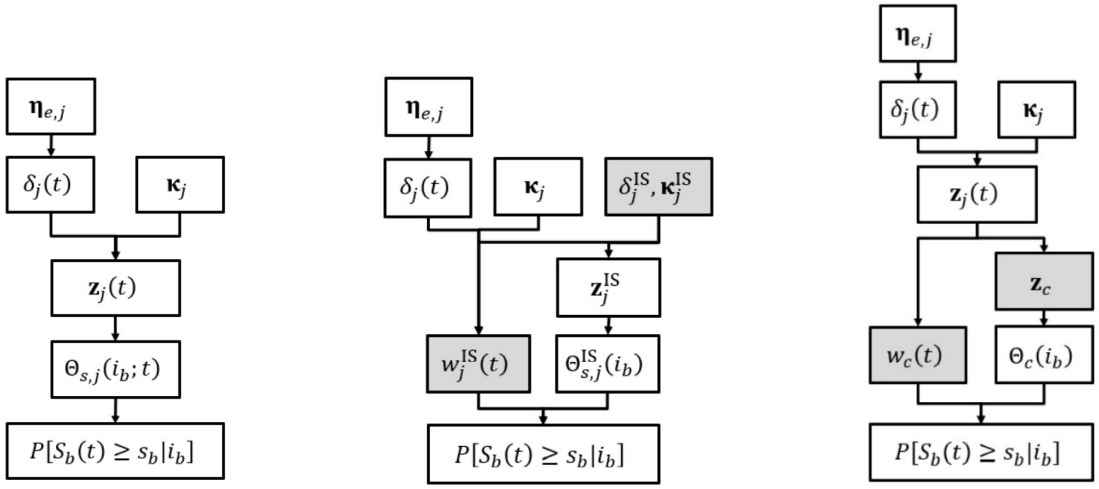

3.2 *Stationary Proposal Importance Sampling (SP-IS)*

The accuracy of the numerical estimate can be largely improved by reformulating the failure probability relying on the definition of an alternative distribution $\psi\mathbf{z}(\mathbf{z})$, referred to as sampling distribution or proposal distribution or Importance Sampling (IS) distribution (Melchers 1989).

A novel Stationary Proposal Importance Sampling (SP-IS) is presented for application to time-variant reliability problems. Figure 1b shows the flowchart of the proposed SP-IS methodology for life-cycle seismic fragility assessment. The time-variant probability of failure can be reformulated as follows:

$$p_f(t) = \int_{\mathbf{z}} I_s[\mathbf{z}] \cdot f_{\mathbf{Z}(t)}(\mathbf{z}) \frac{\psi_{\mathbf{Z}}(\mathbf{z})}{\psi_{\mathbf{Z}}(\mathbf{z})} d\mathbf{z} \quad (8)$$

The estimate of the failure probability is then formulated as the expected value of the weighted indicator function:

$$\hat{p}_{\mathrm{IS}}(t) = \frac{1}{n}\sum_{j=1}^{n} I_s[\mathbf{z}_j] \cdot w_j(t) \quad (9)$$

where the weighting coefficient for the j-th sample $w_j(t)$ is defined as the ratio between the actual PDF $f_{\mathbf{Z}(t)}$ and the sampling PDF $\psi\mathbf{z}$ evaluated in $\mathbf{z}_j$:

$$w_j(t) = \frac{f_{\mathbf{Z}(t)}(\mathbf{z}_j)}{\psi_{\mathbf{Z}}(\mathbf{z}_j)} \quad (10)$$

It is worth mentioning that a drawback of IS-based methods can be encountered in the "curse of dimensionality", since such methods tends to provide inefficient estimates of the failure probability when a large number of basic random variable are involved in the sampling procedure (Au and Beck 2003).

3.3 *Clustering-based data reduction techniques*

A similar approach to Importance Sampling can be adopted exploiting data-reduction techniques, such as data clustering methods. Cluster analysis consists in dividing data into groups sharing similar properties. Clustering can be used for data reduction to develop small catalogs of models heuristically representative of broader groups of data. For example, K-means clustering has been adopted in Jayaram and Baker (2010) for lifeline risk assessment of a large-scale transportation network.

A clustering-based technique is proposed for time-variant reliability problems. Figure 1c presents a synthetic flowchart of the proposed technique for life-cycle seismic fragility assessment. This methodology consists in grouping into subspaces $\mathbf{Z}_c$ the sample structural models $z_j(t)$ simulated throughout the lifetime of the deteriorating system. Structural analyses are then carried out on a single structural model per cluster

associated with the centroid $\mathbf{z}_c$ of each subspace $\mathbf{Z}_c$, representative of the response of any structural model within the cluster. Finally, the time-variant failure probability estimate is obtained by weighting the indicator function of each failed sample by the time-variant observation frequency of samples within each cluster:

$$\hat{p}_{\mathrm{CLST}}(t) = \frac{1}{n_c}\sum_{c=1}^{n_c} I_s[\mathbf{z}_c] \cdot w_c(t) \quad (11)$$

where the weighting coefficient for the c-th sample $w_c(t)$ is estimated as the time-variant sample frequency of the cluster based on the simulated structural models $\mathbf{z}_j(t)$:

$$w_c(t) = \frac{1}{n_j}\sum_{j=1}^{n_j} I\left[\mathbf{z}_j(t) \in \mathbf{Z}_c\right] \quad (12)$$

4 APPLICATIONS

4.1 *Lifetime collapse reliability of a beam*

The collapse analysis of a beam is presented as a benchmark for time-variant reliability analysis (Biondini 2008). Figure 2 shows the collapse mechanism and the bending moment diagram at collapse of a beam of total length $2l$=6m loaded at midspan by a concentrated force ΘQ considering perfect plasticity with plastic bending moment M_p.

The time-variant collapse probability is expressed as follows:

$$p_f(t) = P[\Theta(t) \le 1] \quad (13)$$

where the collapse load multiplier is the safety factor with respect to beam failure:

$$\Theta(t) = \frac{3M_p(t)}{Ql} \quad (14)$$

By assuming l as deterministic, if both Q and M_p are statistically independent lognormal random variables, the collapse load multiplier Θ is also lognormal (Ang and Tang 2007). The statistical descriptors of load Q and moment M_p are listed in Table 1. The loading is assumed to be independent on time, whilst the plastic moment is characterized by linearly decaying mean $\mu_M(\tau)$ and linearly increasing CoV $\delta_M(\tau)$ in terms of the time variable $\tau=t/t_h$ expressing the time instant t normalized to a given horizon time t_h.

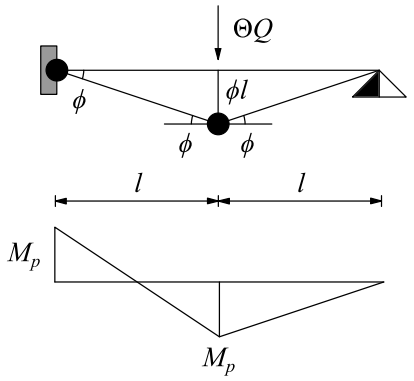

Table 1. Statistical descriptors of the time-variant lognormal independent random variables Q and M_p.

Random Variable	Load Q	Moment M_p
Mean Value μ	100 kN	(1-τ/3)·210 kNm
CoV δ	0.12	0.15+0.15τ

These functions are chosen to simulate severe deterioration progressively reducing the expected beam capacity and increasing its variability. The reliability index under these assumptions can be evaluated analytically. The initial value $\beta(t=0)$=3.86 decays over time to $\beta(t=t_h)$=0.94 as shown in Figure 3.

This solution is compared with the time-variant reliability index estimated using simulation-based techniques. Based on the marginal distributions f_Q and $f_{M_p(t)}$, sampling both the load Q and moment $M_p(t_k)$ at different instants t_k allows evaluating the distribution of the sample safety factor. The MCS failure probability estimate is obtained as follows:

$$\hat{p}_{\mathrm{MCS}}(t_k) = \frac{1}{n_j}\sum_{j=1}^{n_j} I\left[\frac{3}{l}\frac{m_j(t_k)}{q_j} \le 1\right] \quad (15)$$

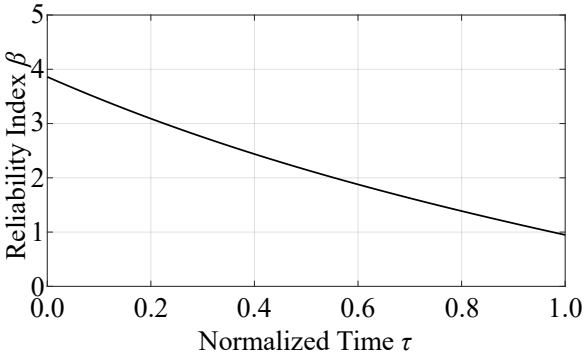

Figure 3. Time-variant reliability index.

Importance Sampling can be adopted to improve the accuracy of the reliability estimates by simulating Q and M_p based on alternative proposal distributions. The sample set is generated based on lognormal statistically independent proposal distributions Q and M_p with descriptors collected in Table 2. Since the safety factor Θ is inversely proportional to Q, the mean value of the concentrated force has been increased from 100 to 120 kN, inflating the likelihood of sampling more severe though unlikely load demands that may lead to failure. Conversely, since Θ is directly proportional to M_p, the mean value has been set equal to 100 kNm whilst the actual time-variant mean value $\mu_M(t)$ linearly varies from 210 to 140 kNm. The coefficients of variation of the proposal marginal distributions of moment M_p and load Q have also been raised to 0.30, increasing the likelihood of sampling values of both RVs far from their respective central values.

Based on the generation of n_j^{IS} samples, the IS estimate of the time-variant failure probability is obtained as follows:

$$\hat{p}_{IS}(t_i) = \frac{1}{n_j^{IS}} \sum_{j=1}^{n_j^{IS}} I\left[\frac{3}{l}\frac{m_{p,j}}{q_j} \le 1\right] \cdot w_j(t_k) \quad (16)$$

where the time-variant weighting coefficients $w_j(t_k)$ depend on the actual and proposal distributions as follows:

$$w_j(t) = \frac{f_Q(q_j)}{\psi_Q(q_j)} \cdot \frac{f_{M_p(t)}(m_j)}{\psi_{M_p}(m_j)} \quad (17)$$

Figure 4 shows the scatterplots with $5 \cdot 10^5$ samples of MCS simulation for τ=0.0, 0.5, and 1.0 (in gray scale with increasing shades, Figures 4a,b,c), and for the IS simulation regardless of the reference time (Figure 4d). In each scatterplot, the line represents the limit state function separating the sample set into failure domain (below) and safe domain (above). The MCS samples tend to migrate along the ordinate due to the progressive reduction of the mean plastic moment μ_M and increase of its CoV δ_M. Unlike crude time-variant MCS, the IS samples are time-invariant since the proposal distribution does not depend on τ.

Table 2. Statistical descriptors of the proposal lognormal independent distributions for Q and M_p.

Random Variable	Load Q	Moment M_p
Mean Value μ	120 kN	100 kNm
CoV δ	0.30	0.30

Figure 5 shows the evolution in time of the reliability index estimates computed by crude MCS simulation (in blue) and the proposed IS approach (in red). The estimates are compared with the exact solution (horizontal dashed black lines). The accuracy of both estimates intuitively increases with the number of simulations, but the IS estimate shows good agreement with the exact one after about 10^3 samples.

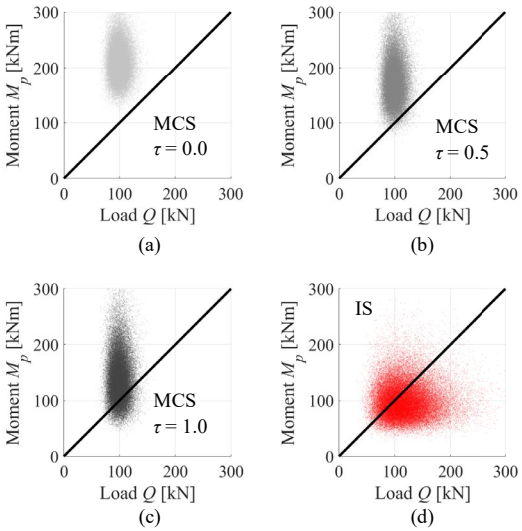

Figure 4. Scatterplots of MCS samples generated at (a) t_k=0, (b) t_k=0.5t_h, (c) t_k=t_h, and (d) IS samples generated from the proposal distribution.

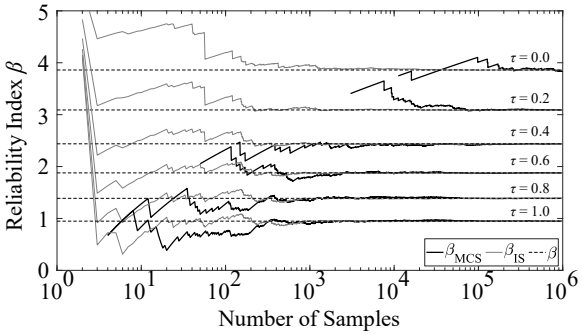

Figure 5. MCS and IS estimates of the time-variant reliability index vs. the sample size at different times.

Furthermore, the CoV of the failure

probability estimate obtained via crude MCS increases with the value of β to be estimated, as made evident in the results for different values of τ. Conversely, the accuracy of IS estimates is not significantly affected at different time instants.

The rate of convergence of MCS and IS is also shown in Figure 6, which represents the time evolution of the percentage error in the reliability estimates with 10^6 samples in comparison with the exact solution. The results confirm the trend observed in Figure 5: the IS estimate is providing a maximum percentage error of about 0.02%, whilst the MCS estimate floats in time with a positive trend due to the larger accuracy of the method in evaluating larger and larger failure probabilities and, in turn, smaller and smaller reliability indices. Other quantitative metrics of the estimate accuracy could be defined based on the statistical estimators of the variance of the failure probability (Melchers and Beck 2018, Capacci and Biondini 2021).

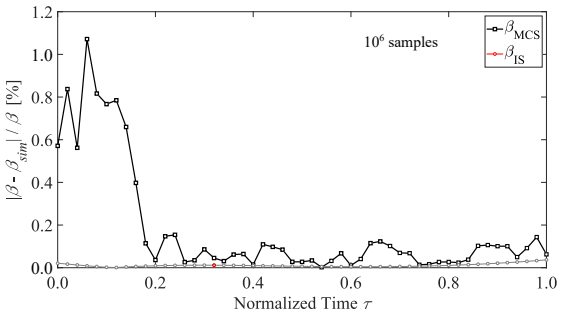

Figure 6. Time-variant normalized error of reliability estimates based on MCS and IS sampling approaches.

4.2 *Lifetime seismic fragility of a RC bridge*

The time-variant seismic fragility of the three-span continuous RC bridge shown in Figure 7 is investigated (Bouassida et al. 2012, Capacci 2020). The bridge piers are exposed to a chloride diffusive attack on the with concentration C_s. The concrete cover is 60mm. Each reinforcing steel bar suffers the same chloride-induced corrosion process. The percentage of steel mass loss δ_s of the bars is hence assumed as representative of the damage effects suffered by the bridge.

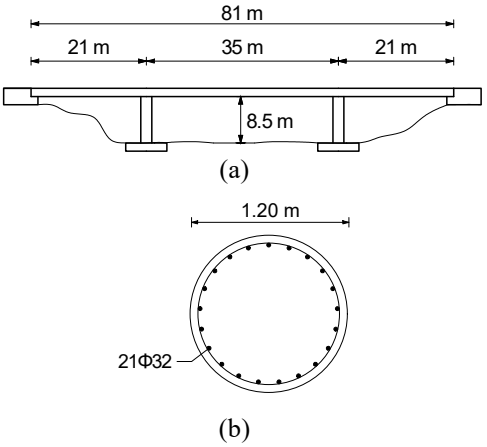

Figure 7. RC bridge: (a) main geometrical dimensions and (b) cross-section of the piers.

The 1D Fick's diffusion equation is used to assess the corrosion initiation time t_{cr}:

$$C(x,t) = C_s \cdot \left[1 - \mathrm{erf}\left(\frac{x}{2\sqrt{D(t)\cdot t}}\right)\right] \quad (18)$$

with concrete diffusivity $D(t)$ defined in terms of reference diffusivity coefficient D_e, aging coefficient a, and annual average temperature T [°C] (Stewart et al. 2011):

$$D(t) = D_e \left(\frac{0.076}{t}\right)^a \exp\left[\frac{40}{8.314\times10^{-3}}\left(\frac{1}{293} - \frac{1}{273+\bar{T}}\right)\right] \quad (19)$$

After corrosion onset at time t_{cr}, the deterioration δ_s is evaluated based on the corrosion rate expressed in terms of current density i_{corr} [μA/cm^2], pristine bar diameter ϕ_0 [mm], and pitting factor R_f:

$$\delta_s(t) = \frac{0.0116 R_f}{\phi_0} \cdot \int_{t_{cr}}^{t} i_{corr}(t)dt \quad (20)$$

The current density is related to temperature T based on a reference current density at T=20°C, i.e. $i_{corr,20}$, as follows:

$$i_{corr}(t) = i_{corr,20}\{1 + K[T(t) - 20]\} \quad (21)$$

where and the scale coefficient K is equal to 0.025 and 0.073 for T<20°C and T>20°C, respectively. The temperature profile $T(t)$ is defined by simulating seasonal temperature variations around an average temperature $\bar{T} = 15°C$ by sinusoidal functions with amplitude dependent on hot and cold seasons assumed to have 50%-50% duration with maximum and minimum temperatures T_{min}=5°C and T_{max}=25°C, respectively (Bastidas-Arteaga et al. 2013).

Damage state exceedance for the bridge system $\mathbf{Z}$ is associated with the attainment of progressively restrictive conditions on the maximum response curvature χ_b at the base of the bridge piers, informative of the accumulation of excessive plastic strains in critical regions after the occurrence of the k-th ground motion of intensity i_b. Fragility analysis is based on the following factor:

$$\Theta_s[\mathbf{Z}(t)|i_b] = \frac{\chi_b[\mathbf{Z}(t),i_b]}{\bar{\chi}_s[\mathbf{Z}(t)]} \quad (22)$$

where $\bar{\chi}_s$ is the capacity threshold of the s-th limit state. The four limit states listed in Table 3 are considered, where the capacity thresholds are based on first yielding curvature χ_y, plastic curvature $\chi_p=\chi_u-\chi_y$, and ultimate curvature χ_u.

Table 3. Bridge pier curvature capacity thresholds.

Damage State	Limit Curvature $\bar{\chi}_s$
Slight Damage s=1	χ_y
Moderate Damage s=2	χ_y +0.3χ_p
Extensive Damage s=3	χ_y +0.6χ_p
Nominal Collapse s=4	χ_u

Model uncertainties are considered by modeling the parameters of chloride exposure, corrosion rate, and mechanical properties as random variables with distributions and parameters collected in Table 4. Concerning the record-to-record variability, a set of 20 artificial ground motions compliant with the elastic response spectrum given by Eurocode 8 for soil type B is considered (CEN-EN 1998-1: 2004).

The steel damage index δ_s is considered as the only random variable sampled based on a stationary proposal distribution. A mixed proposal distribution is assumed: 65% of the realizations are non-null and non-unitary damage indices sampled from a standard beta distribution with parameters α=0.8 and β=1.5; no damage and full damage conditions are associated with discrete probabilities $P[\delta_s=0]$=30% and $P[\delta_s=1]$=5%, respectively. Figure 8 shows the overall CDF of the proposal distribution for the damage index (in red) compared with the actual time-variant CDF.

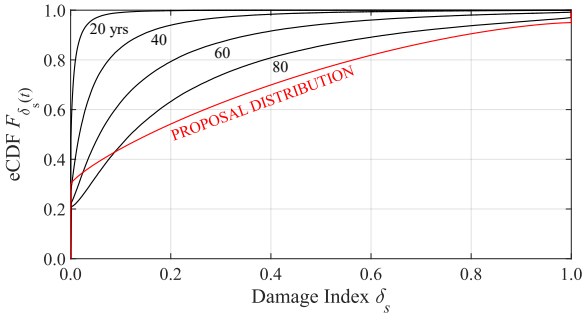

Figure 8. Stationary proposal distribution (red line) and empirical CDFs (black line) of the steel damage index δ_s at different times (Δt=20 years).

The corrosion effects in terms of reinforcing steel bar cross-section reduction, ultimate steel strain ε_{su}, and concrete cover compressive strength f_c are related to the damage index δ_s based on the model proposed in Biondini and Vergani (2015). The time-variant structural capacity of the deteriorating bridge piers is evaluated in terms of bending moment M vs curvature χ. The capacity curves linearized at cracking, yielding and ultimate are presented in Figure 9 for at different time instants and different simulation techniques.

Figure 9a shows 10^4 $M-\chi$ relationships calibrated at time t=0, i.e., when corrosion is not yet initiated and $\delta_{s,j}$=0 $\forall j$. The transparency of each line is increased to graphically perceive the variation in time of the occurrence frequency of different $M-\chi$ trends. Then, given the simulation of the damage index δ_s at prescribed time instants, it is possible to evaluate the impact of chloride-induced corrosion. The simulation is performed to evaluate $M-\chi$ relationships every ten years from the pristine condition up to 80 years, for a total number of time instants n_t=9.

As an example, Figure 9b shows the linearized $M-\chi$ relationships at times t=80 years. Progressive deterioration severely impairs the mechanical properties of the piers cross-section in terms of strength and ductility, respectively due to the steel mass loss and ultimate steel strain reduction. Also, the cross-section stiffness is slightly reduced, mainly due to concrete cover strength reduction up to spalling.

Table 4. Probabilistic distribution type and descriptors of the basic random variables.

Random Variable	Type	μ	σ
Initial Concentration C_s [%wt./c]	Truncated Positive Normal	3.0	0.30 μ
Reference Diffusivity D_e [10^{-12}m^2/year]	Truncated Positive Normal	15.8	0.20 μ
Aging Parameter a [-]	Uniform Beta	0.30	0.12
Critical Concentration C_{cr} [%wt./c]	Beta bounded in [0.2-2.0]	0.60	0.15
Current Density at 20°C $i_{corr,20}$ [μA/cm^2]	Lognormal	2.586	1.724
Pitting Factor R_f [-]	Gumbel	7.1	0.17
Concrete Strength f_c [MPa]	Lognormal	38	5
Steel Strength f_y [MPa]	Lognormal	500	30

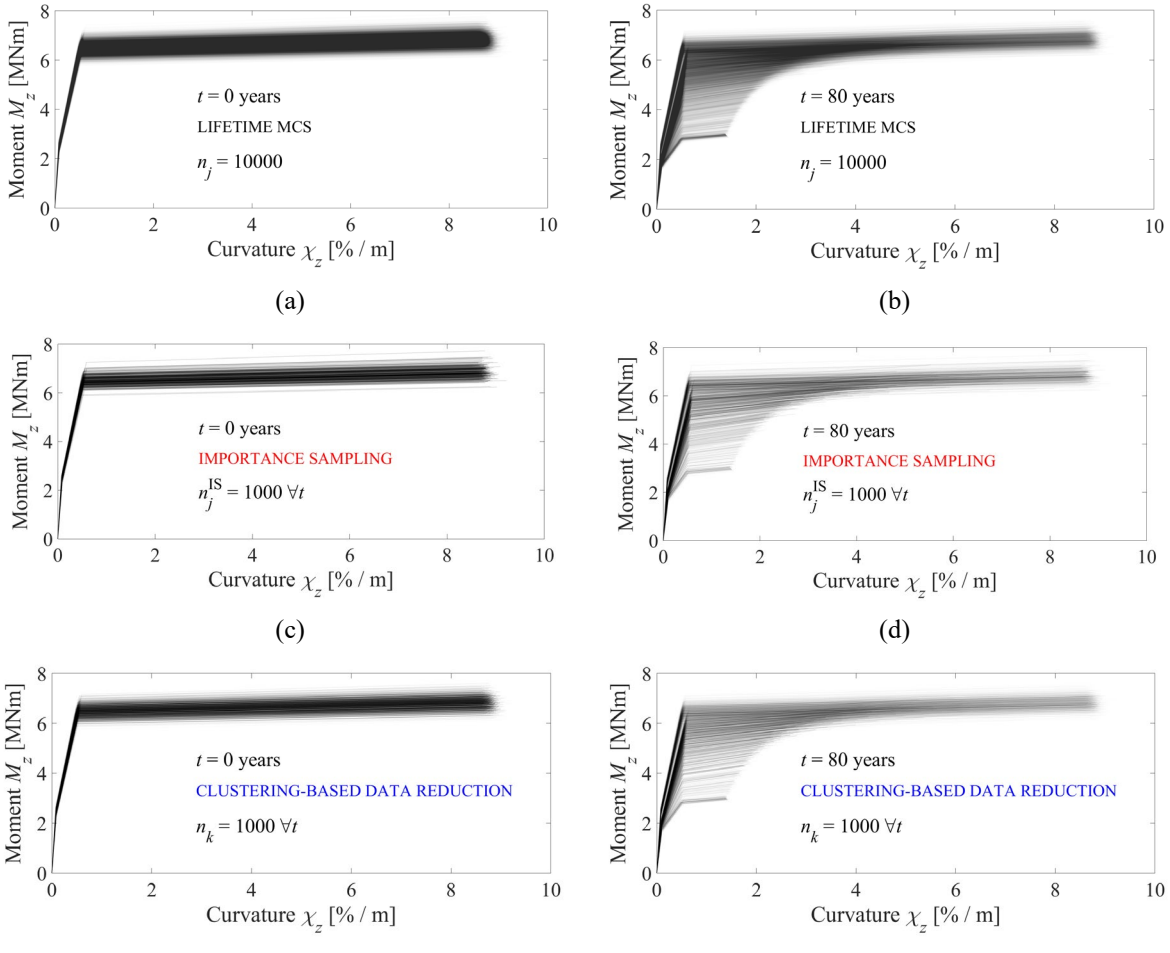

Figure 9. Lifetime linearized moment-curvature relationships at (a,c,e) t=0, (b,d,f) t=80 years based on (a,b) Monte Carlo simulation, (c,d) Stationary Proposal Importance Sampling, and (e,f) data reduction technique.

The SP-IS approach is used to generate n_j=10^3 mechanical parameters and steel damage indices to obtain the samples of M–χ relationships shown in Figure 9c,d for t=0 (Figure 9c) and t=80 years (Figure 9d). The transparency of each sample backbone curve depends on the time-variant IS weighting coefficient $w_j(t)$. In crude MCS, the structural performance decay is simulated at each time step, whilst in the SP-IS approach it is accounted for by the time-variant weighting coefficient.

Concerning a clustering-based approach, K-means clustering is adopted to reduce the catalog down to n_c=10^4 M–χ capacity curves. This technique groups the data into

n_c clusters by progressively minimizing the dissimilarity between each observation and the centroid $\mathbf{z}_c$ of the cluster $\mathbf{Z}_c$. The centroids are initially selected randomly, and the observations are assigned to the cluster with the closest centroid with respect to a suitable norm. After the initial assignment, an iterative procedure allows updating each centroid $\mathbf{z}_c$ in the model parameters space and the subsequent re-assigning all observations to the cluster with the closest centroid.

Within this framework, a catalog of $n_t \cdot 10^4 = 9 \cdot 10^4$ simulations have been computed for moment-curvature pairs $[M,\chi]_i$ at cracking (i=1), yielding (i=2) and ultimate (i=3). The Euclidean norm is used for the six modeling parameters, namely $[M,\chi]_i$ with i=1,2,3. The reduced backbone M–χ catalog is reported in Figure 9e,f with varying line transparency depending on the occurrence frequency of observations within the related cluster at times t=0 (Figure 9e) and t=80 years (Figure 9f). The comparison between graphs in Figure 9a,c,e and Figure 9b,d,f allow appreciating the same decreasing trend in cross-section strength and ductility across all applied methodologies.

Time-variant seismic fragility analysis of the corroding RC bridge under ground motion is carried out based on multi-stripe non-linear dynamic analyses. The structural model consists of linear elastic beam elements for the bridge deck and nonlinear beam elements with lumped plasticity for the bridge piers. The lumped plasticity model is built on the computed time-variant M–χ capacity curves. The acceleration time-histories is scaled over six levels of peak ground acceleration (PGA), namely from 0.2g to 1.2g with steps of 0.2g. Figure 10 allows comparing the failure probability associated to different limit states estimated with traditional MCS (black dots), SP-IS approach (red squares), and clustering-based technique (blue diamonds). The results for both SP-IS and clustering-based methodologies based on the analyses of 10^3 structural models are providing failure estimates similar to crude MCS based on $n_t \cdot 10^4$ models investigated.

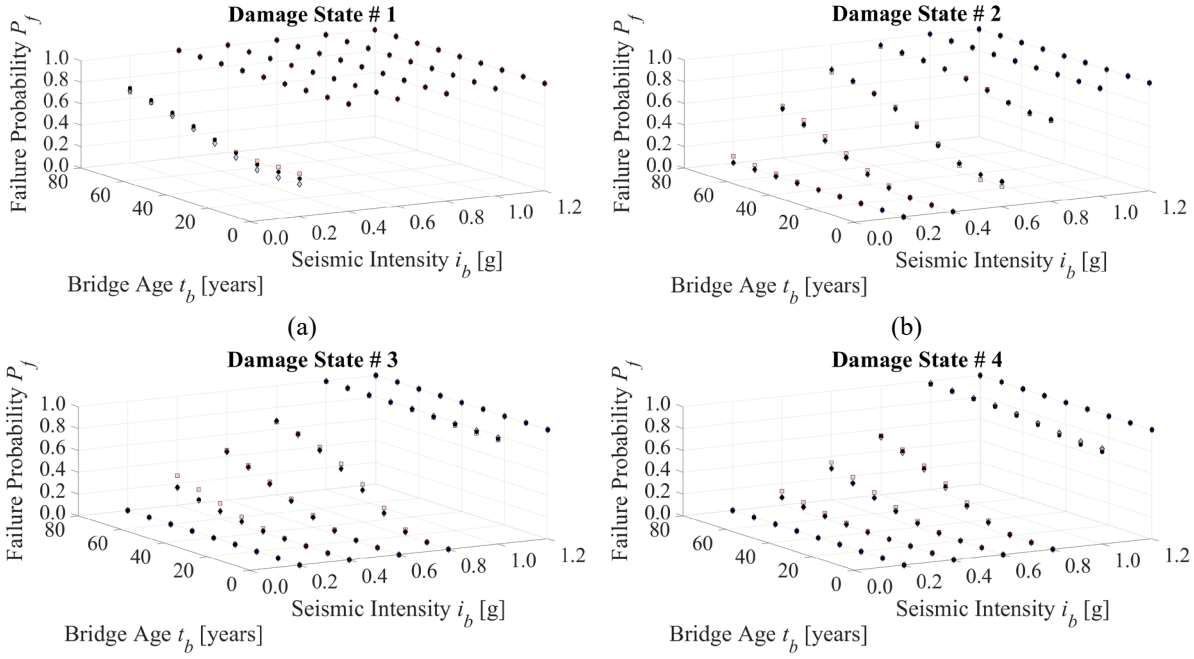

Figure 10. Failure probability estimates with traditional MCS (black dots), SP-IS (red squares), and clustering-based technique (blue diamonds) every 10 years for limit states (a) s_b=1, (b) s_b=2, (c) s_b=3, and (d) s_b=4.

5 CONCLUSIONS

Novel computational approaches based on importance sampling and data reduction techniques have been proposed to efficiently estimate the time-variant failure probability of deteriorating structures. Structural systems are simulated to account for the time-variant modeling uncertainties typical of life-cycle reliability problems. The methodologies have been validated on a simple benchmark and applied to the time-variant seismic fragility assessment of a RC bridge under corrosion. The potentiality of the proposed methods emerges when time-consuming analyses are required to investigate the structural response of systems characterized by a limited number of time-variant constitutive parameters.

Convergence criteria based on sensitivity analysis are necessary to better identify boundaries and advantages for sample size selection (Capacci and Biondini 2021). Further research should be devoted to calibrating optimal proposal distributions and data reduction strategies and to evaluating feasibility limitations in time-variant risk-based assessment of aging large-scale structures (Messore et al. 2021).

REFERENCES

Ang, A.H.S. & Tang, W.H. 2007. *Probability concepts in engineering*, Hoboken, NJ: Wiley.

Au, S.K. & Beck, J.L. 2003. Importance sampling in high dimensions. *Structural Safety*, 25(2): 139–163.

Bastidas-Arteaga, E., Schoefs, F., Stewart, M.G., & Wang, X. 2013. Influence of global warming on durability of corroding RC structures: a probabilistic approach. *Engineering Structures*, 51, 259–266.

Biondini, F. 2008. Use of simulation in structural reliability, *Structures Congress 2008*, ASCE, Vancouver, BC, Canada, April 24-26, 2008.

Biondini, F. & Frangopol, D.M., 2016. Life-cycle performance of deteriorating structural systems under uncertainty: Review, *Journal of Structural Engineering*, ASCE, 142(9), F4016001, 1-17.

Biondini, F. & Vergani, M., 2015. Deteriorating beam finite element for nonlinear analysis of concrete structures under corrosion. *Structure and Infrastructure Engineering*, 11(4), 519-532.

Bouassida, Y., Bouchon, E., Crespo, P., Croce, P., Davaine, L., Denton, S., Feldmann, M., Frank, R., Hanswille, G., Hensen, W., Kolias, B., Malakatas, N., Mancini, G., Ortega, M., Raoul, J., Sedlacek, G., & Tsionis, G. 2012. *Bridge design to Eurocodes. Worked examples.* JRC Scientific and Technical Reports, EUR 25193 EN-2012.

Capacci, L. 2020. *Life-cycle seismic resilience of aging bridges and infrastructure networks*. PhD Thesis, Politecnico di Milano, Milan, Italy.

Capacci, L. & Biondini, F., 2020. Probabilistic life-cycle seismic resilience assessment of aging bridge networks considering infrastructure upgrading. *Structure and Infrastructure Engineering*, 16(4), 659–675.

Capacci, L. & Biondini, F. 2021. Importance sampling in life-cycle seismic fragility and risk assessment of aging bridge networks. *1st Conference of the European Association on Quality Control of Bridges and Structures* (EUROSTRUCT 2021), Padova, August 29th-September 1st, 2021.

Capacci, L., Biondini, F., & Titi, A. 2020. Lifetime seismic resilience of aging bridges and road networks. *Structure and Infrastructure Engineering*, 16(2), 266–286.

CEN-EN 1998-1: 2004. *Eurocode 8: Design of Structures for Earthquake Resistance*, European Committee for Standardization, Brussels.

Ellingwood, B.R., 2005. Risk-informed condition assessment of civil infrastructure: state of practice and research issues. *Structure and Infrastructure Engineering*, 1(1), 7-18.

Ghosn, M., Dueñas-Osorio, L., Frangopol, D.M., McAllister, T. P., Bocchini, P., Manuel, L., Ellingwood, B.R., Arangio, S. Bontempi, F., Shah, M., Akiyama, M., Biondini, F., Hernandez, S., & Tsiatas, G. 2016. Performance indicators for structural systems and infrastructure networks. *Journal of Structural Engineering*, ASCE, 142(9), F4016003.

Jayaram, N. & Baker, J.W. 2010. Efficient sampling and data reduction techniques for probabilistic seismic lifeline risk assessment. *Earthquake Engineering & Structural Dynamics*, 39:1109–1131.

Melchers, R.E. 1989. Importance sampling in structural systems. *Structural Safety*, 6(1), 3-10.

Melchers, R.E. & Beck, A.T. 2018. *Structural reliability analysis and prediction*. John Wiley & Sons.

Messore, M.M., Capacci, L., & Biondini, F. 2021. Life-cycle cost-based risk assessment of aging bridge networks. *Structure and Infrastructure Engineering*, 17(4), 515-533.

Silva, V., Akkar, S., Baker, J.W., Bazzurro, P., Castro, J.M., Crowley, H., Dolsek, M., Galasso, C., Lagomarsino, S., Monteiro, R., Perrone, D., Pitilakis, K., & Vamvatsikos, D. 2019. Current challenges and future trends in analytical fragility and vulnerability modelling. *Earthquake Spectra*, 35(4), 1927-1952.

Stewart, M.G., Wang, X., & Nguyen, M.N. 2011. Climate change impact and risks of concrete infrastructure deterioration. *Engineering Structures*, 33, 1326–1337.